NASA TECHNICAL NOTE

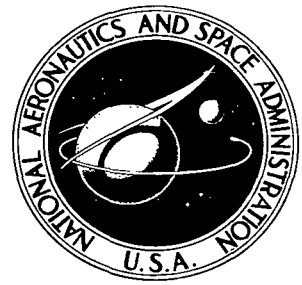

NASA TN D-6023

NASA TN D-6023

EFFECTS OF NATURAL CHEMICAL IMPURITIES AND CRYSTALLITE ORIENTATION ON THE EROSION BEHAVIOR OF ARTIFICIAL GRAPHITE

by Howard G. Maahs

Langley Research Center
Hampton, Va. 23365

NATIONAL AERONAUTICS AND SPACE ADMINISTRATION • WASHINGTON, D. C. • NOVEMBER 1970

1. Report No.	2. Government Accession No.	3. Recipient's Catalog No.
NASA TN D-6023		

4. Title and Subtitle
EFFECTS OF NATURAL CHEMICAL IMPURITIES AND CRYSTALLITE ORIENTATION ON THE EROSION BEHAVIOR OF ARTIFICIAL GRAPHITE

5. Report Date: November 1970

6. Performing Organization Code:

7. Author(s): Howard G. Maahs

8. Performing Organization Report No.: L-6792

9. Performing Organization Name and Address:
NASA Langley Research Center
Hampton, Va. 23365

10. Work Unit No.: 129-03-18-06

11. Contract or Grant No.:

12. Sponsoring Agency Name and Address:
National Aeronautics and Space Administration
Washington, D.C. 20546

13. Type of Report and Period Covered: Technical Note

14. Sponsoring Agency Code:

15. Supplementary Notes:

16. Abstract

The effects of natural chemical impurities and crystallite orientation on the erosion behavior of several artificial graphites have been determined in a Mach 2 airstream with a stagnation-point pressure of 5.6 atm and a nominal total enthalpy of 2.27 MJ/kg. The presence of natural chemical impurities caused higher surface temperatures and erosion rates, whereas differences in crystallite orientation had little effect on erosion rate provided the surface temperatures for the different orientations were the same. However, since the thermal conductivity of graphite depends on crystallite orientation, the surface temperatures of those graphites tested while contacting a heat sink varied with orientation. Higher temperatures were attained by the graphites when the across-grain direction of the graphite was in contact with the heat sink; accompanying these higher temperatures were higher erosion rates. Because the observed erosion rates were much slower than diffusion-control predictions and, in addition, were a function of surface temperature, it was reasoned that erosion was not controlled solely by diffusion but that reaction kinetics was still playing an important role in determining erosion rate.

17. Key Words (Suggested by Author(s))	18. Distribution Statement
Graphite erosion Graphite, chemical impurities Graphite, crystallite orientation Graphite ablation	Unclassified – Unlimited

19. Security Classif. (of this report)	20. Security Classif. (of this page)	21. No. of Pages	22. Price*
Unclassified	Unclassified	33	$3.00

*For sale by the Clearinghouse for Federal Scientific and Technical Information
Springfield, Virginia 22151

EFFECTS OF NATURAL CHEMICAL IMPURITIES AND CRYSTALLITE ORIENTATION ON THE EROSION BEHAVIOR OF ARTIFICIAL GRAPHITE

By Howard G. Maahs
Langley Research Center

SUMMARY

The effects of natural chemical impurities and crystallite orientation on the erosion behavior of several artificial graphites have been determined in a Mach 2 airstream with a stagnation-point pressure of 5.6 atm and a nominal total enthalpy of 2.27 MJ/kg. The parameters selected for assessing the erosion behavior of the graphites were total recession for a given test duration Δl, linear stagnation-point mass loss rate $\dot{m}$, and stagnation-point surface temperature T_s.

Some of the graphites tested eroded evenly with smooth aftertest surfaces, whereas others eroded unevenly, with rough, pitted surfaces. For those graphites which eroded evenly, the presence of natural chemical impurities had the effect of producing higher values of Δl, $\dot{m}$, and T_s. For those graphites which eroded unevenly, the effects of natural chemical impurities were qualitatively similar but not as large.

Crystallite orientation proved to have little effect on erosion behavior provided T_s for the different orientations was the same; however, since the thermal conductivity of graphite depends on its crystallite orientation, T_s varied with orientation for a given graphite specimen when the specimen was tested in contact with a heat sink. Higher values of T_s were attained when the across-grain direction of the graphite was in contact with the heat sink. Accompanying these higher values of T_s were higher values of Δl and $\dot{m}$. These effects were observed for those graphites which eroded evenly; for those graphites which eroded unevenly, there was no discernible effect of orientation on T_s, Δl, or $\dot{m}$ even when the specimen was tested in contact with a heat sink.

For any given graphite and impurity level, $\dot{m}$ was found to be a function of T_s alone, being virtually independent of crystallite orientation, level of heat flux, and thermal conduction from the specimen. Because of this dependence of erosion rate on surface temperature, it was reasoned that the erosion process was not controlled solely by the diffusion of oxygen to the reacting surface.

The graphite erosion rates obtained in this study are much slower than oxidation rates predicted by some commonly accepted kinetic models and, in addition, are even

slower than diffusion-control predictions. Furthermore, the apparent activation energy calculated for the erosion process is approximately 1/3 to 1/6 of the activation energies commonly reported for oxidation. One possible explanation for both of these results is that at the present test conditions the carbon-oxygen reaction has a lower true activation energy than has often been assumed.

INTRODUCTION

Artificial graphite is a material having recognized utility for many high-temperature applications. One application for which it appears particularly attractive is as a nose tip on reentry vehicles, particularly for those encountering the higher stagnation pressures at which charring ablators lack sufficient mechanical integrity. Artificial graphite is, however, not one single material but is representative of an entire class of industrially manufactured carbonaceous materials. Specifically, the term "artificial graphite" conventionally refers to the common, commercially manufactured graphite composed of a carbon filler phase held together with a carbonized binder phase, which mixture has been graphitized as one body. Because of the wide variations in formulation and manufacturing techniques, artificial graphites vary considerably in their chemical, structural, thermophysical, and mechanical properties. These properties include, among others, the concentration of natural chemical impurities and the degree of preferential crystallite orientation.

Changes in either chemical impurity concentration or crystallite orientation or in both could affect the erosion behavior of an artificial graphite. For example, it is well known that the majority of chemical elements, when present in graphite as impurities, accelerate the oxidation rate of the graphite (see, for example, ref. 1). Furthermore, it has been shown that the particular chemical impurities which occur naturally in conventional artificial graphite, when considered as a group, should also accelerate its oxidation rate (ref. 1). Preferential crystallite orientation in artificial graphite has, in addition, been suspected of being an important factor affecting oxidation rate (see, for example, ref. 2). It is recognized, however, that the rate of the oxidation reaction alone does not necessarily determine the rate of total erosion of artificial graphite in a dynamic environment. Mass transport of oxygen to the reacting surface, sublimation, mechanical removal of fine particulate matter or grains, and spallation may also contribute. Consequently, the extent to which natural chemical impurities and crystallite orientation of artificial graphite affect its erosion rate or, more generally, its overall performance in a dynamic environment is not known.

The present investigation was undertaken to determine experimentally the magnitude of the effects, if any, which natural chemical impurities and crystallite orientation have

on the erosion behavior of artificial graphite in a representative reentry environment. In this report are presented the results of this experimental study. The parameters selected for assessing this behavior were total recession for a given test duration, linear stagnation-point mass loss rate, and stagnation-point steady-state surface temperature. The dynamic test environment was a Mach 2 airstream with a stagnation-point pressure of 5.6 atm and a nominal total enthalpy of 2.27 MJ/kg. Heating rates were nominally 540 W/cm^2.

SYMBOLS

Δl total specimen length change resulting from 30-second exposure to test environment, cm

$\dot{m}$ linear mass loss rate at stagnation point, g/cm^2sec

$\dot{m}_D$ diffusion-controlled stagnation-point mass loss rate for 0.635-cm-nose-radius body, g/cm^2sec

q_{cw} stagnation-point cold-wall heating rate (cold-wall temperature, 333° K), W/cm^2

T_s stagnation-point surface temperature at steady state, $^\circ K$

Other notation:

A/G across grain

Pure specially purified form

Std standard (impure) form as conventionally supplied by manufacturer

W/G with grain

EXPERIMENTAL EQUIPMENT AND PROCEDURE

Test Environment

The test environment consisted of a nominal Mach 2 airstream with a nominal total enthalpy of 2.27 MJ/kg and a stagnation pressure of 5.6 atm. Heating rates were nominally 540 W/cm^2. This test environment was obtained in the Langley arc-heated

materials jet described in reference 3. Stagnation pressures and heating rates in the test stream were measured with a calibrated pressure probe and a calibrated Gardon foil asymptotic calorimeter, respectively. Stream enthalpy was calculated using the Fay and Riddell equation (ref. 4).

Test Specimens

The graphite test specimens, shown schematically in figure 1, were machined from graphite billets as supplied by the manufacturer. The specimens were 1.270-cm-diameter hemisphere-cylinders, 1.905 cm long with nose radii of 0.635 cm. During an ablation test the specimens were mounted either directly in a water-cooled holder or in a 1.905-cm-long phenolic-asbestos insulator which was in turn mounted in the water-cooled holder (see fig. 1). In several tests in which the specimens were mounted directly in the water-cooled holder, a small gap was set between the base of the specimens and the front face of the holder so that the specimens and the holder were in poor thermal contact.

A list of the graphites studied, along with selected properties of each, is given in table I. These several graphites were selected to represent a range in density and maximum grain size and two different filler carbons. In order to study the effect of natural chemical impurities, four of these graphites were obtained from the manufacturer in a specially purified form in addition to the conventionally supplied form; throughout this report these forms are referred to as "purified" and "standard," respectively. Purification was reportedly accomplished by high-temperature halogenation of the standard form of the graphite. The ash content and total impurity content of the graphites studied were determined as described in reference 1. A breakdown of the total chemical impurities in each of these graphites into separate chemical elements is also given in reference 1. Filler-carbon type and maximum grain (filler particle) size were furnished by the manufacturer. Bulk density was calculated from the measured dimensions and mass of three accurately machined cylinders selected at random from a billet of each graphite. Anisotropy ratio (a measure of preferential crystallite orientation) was determined by X-ray diffractometry by using the method of Bacon (ref. 5). This ratio is a measure of the relative number of crystallite faces lying in a plane parallel to the across-grain direction of the graphite to those lying in a perpendicular plane (i.e., in the with-grain direction). The ratio has a value of unity when the crystallites in the graphite are completely randomly oriented, and it decreases toward zero as crystallite orientation increases.

Instrumentation and Data Analysis

Instrumentation used for measuring the ablation behavior of the graphite specimens consisted of a bench micrometer (direct reading in inches to 0.0001 inch (0.00025 cm)),

a motion-picture camera with a framing rate of 200 frames/sec, and a continuous-recording photographic pyrometer. (The theory and operation of the pyrometer used is described in reference 6.) The parameters selected for evaluating ablation behavior were total length change Δl resulting from a 30-second exposure to the test environment, linear stagnation-point mass loss rate $\dot{m}$, and steady-state stagnation-point surface temperature T_s. Total length change was obtained from length measurements of the specimen before and after test. Linear mass loss rate was determined from the motion-picture film record of the eroding specimen as follows. Specimen length as a function of time was obtained from the film record of the specimen with the aid of a motion analyzer. These data were then plotted as shown in the sample plot in figure 2. Specimen length showed an initial increase due to thermal expansion of the graphite but soon passed through a maximum and thereafter decreased continuously because of erosion. Mass loss rate was determined over the linear portion of this decrease by multiplying the slope of the curve (obtained from a least-squares fit of the data) by the bulk density of the graphite. Steady-state stagnation-point surface temperature was determined from the motion-picture film record obtained with the photographic pyrometer. Stagnation-point surface temperatures as a function of time were obtained from this record and plotted as shown in figure 2. For determining these temperatures, the emissivity of graphite was taken to be 0.94 (refs. 7 and 8). The representative stagnation-point surface temperature was taken as the steady-state maximum temperature attained during the run. In all cases, this temperature was reached during the linear portion of the length-time curve.

Typical Test Sequence

A typical test sequence proceeded as follows. The magnetically rotated electric-arc air heater was started and 12 seconds were allowed for the arc to stabilize and the test-stream environment to become established. The motion-picture camera and photographic pyrometer were started and the test-stream heating rate was measured. The graphite specimen to be tested was inserted into the stream and allowed to remain for 30 seconds. After retraction of the specimen, a final heating-rate measurement was made. Each event in this sequence was executed automatically and controlled by a preset programer.

RESULTS AND DISCUSSION

Ablation data obtained for the various graphites studied are presented in table II. These data are divided into two groups: those obtained without insulation between the specimen and the water-cooled holder, and those obtained with insulation. The ablation data presented are total recession in 30 seconds Δl, linear mass loss rate $\dot{m}$, and steady-state surface temperature T_s. Crystallite orientation of the graphites is listed

as A/G (across grain) or W/G (with grain) depending on whether the test stream impinging on the hemispherical nose of the test specimens is parallel to the across-grain or the with-grain direction of the graphite. Chemical impurity level is listed as Std (standard, that is, as conventionally supplied) or Pure (specially purified). Also indicated is the cold-wall heating rate q_{cw} at which each graphite was tested. Although attempts were made to maintain the heating rate near 530 W/cm^2 during the various tests, some small variation about this value occurred. In one test series the heating rate was intentionally set at the higher value of 655 W/cm^2.

Two of the graphites tested, CDG and ATL, eroded unevenly and produced rough, pitted surfaces. Because of excessive erosion, most CDG tests were terminated at 20 seconds; these are noted in table II. This roughening behavior of CDG and ATL contrasts with that of the other graphites which eroded smoothly (see fig. 3). The rough, irregular surfaces are caused by the mechanical removal of fairly large-sized particulate matter (very likely filler particle grains) accompanying the thermochemical oxidative removal. Such particle removal is evident from luminous traces observable in the motion-picture film record. The experimental mass loss rates reported in table II for these graphites must be considered as rough approximations only, since these graphites eroded highly unevenly, developed a conical shape, and did not always erode linearly with time. A more thorough discussion of the phenomenon of particle removal can be found in reference 9.

Effects of Natural Chemical Impurities

In figures 4 and 5 are graphically presented the pertinent data from table II which demonstrate the effects of natural chemical impurities on ablation behavior. Figure 4 presents the data for those graphites which were tested while in thermal contact with the water-cooled holder, whereas figure 5 presents the data for those graphites tested while insulated from the holder. In each of these figures, the ablation behavior of the standard and purified forms of the graphites are compared in terms of Δl, $\dot{m}$, and T_s. To rule out the possibility that chemical impurity effects may also depend on crystallite orientation, the graphites were tested in both the A/G and W/G directions and are so identified in the figures.

The effects of natural impurities in those graphites which eroded evenly are seen in figures 4(a) to 4(f) and 5(a) and 5(b). The standard (impure) forms erode at a faster rate and reach higher surface temperatures than the purified forms. These higher erosion rates and surface temperatures can be explained in terms of the catalytic accelerating effect of the impurities on the oxidation rate coupled with the fact that the oxidation reaction of carbon is exothermic: the impurities in the graphite accelerate its oxidation rate with a resulting increase in observed erosion rate. This increased oxidation rate at the

same time causes an increase in heat input to the specimen as a result of the exothermicity of the reaction and thus drives the surface temperature higher. This higher temperature further increases the oxidation rate, which in turn further increases $\dot{m}$ and T_s, and so on, until a steady state is established where $\dot{m}$ and T_s are greater than for the uncatalyzed case. The largest increases noted in this study were about 20 percent for both Δl and $\dot{m}$ and about 10 percent (or 200° K) for T_s. For each graphite, comparison of the data for the A/G direction with that for the W/G direction (e.g., comparison of fig. 4(a) with fig. 4(b)) shows that the effects of impurities on ablation behavior are qualitatively the same independent of crystallite orientation.

The ablation data for those graphites which eroded unevenly are shown in figures 4(g) and 4(h) and 5(c) and 5(d). The effects of impurities are not as clear-cut for these graphites as for the evenly eroding graphites. However, although there are exceptions, as before, the standard (impure) forms tend to erode at a faster rate. Certainly the impure forms reach higher surface temperatures. This result is consistent with the previous statements regarding the exothermic nature of the reaction. Responsible for the greater scatter in the data for Δl and $\dot{m}$ is the fact that some of the erosion is caused by mechanical removal of discrete particles. Such removal is dependent on the graphite microstructure, localized stresses, voids, cracks, and so forth, and hence is unpredictable and erratic. This lack of predictability in Δl and $\dot{m}$ poses few practical problems in reentry applications, however, because in the usual practical situation graphites such as these will have little, if any, usage.

The foregoing results demonstrate that for those graphites tested, the presence of natural chemical impurities increases erosion rate and surface temperature above those which would result if the impurities were not present. Since the type of natural impurities occurring in most artificial graphites is similar (ref. 1), these results may, with some justification, be extended to other graphites as well. Of course, the magnitude of the effects will depend to some degree on the impurity concentration.

One further point warrants discussion. It was mentioned in the section "Experimental Equipment and Procedure" that the purification of the graphites was accomplished by high-temperature halogenation. It may be presumed that the halogen was chlorine. Since chlorine is known to be an effective oxidation inhibitor (ref. 1), the possibility exists that residual chlorine contained in the purified graphites is inhibiting oxidation and that this chlorine is responsible for the lower erosion rates instead of the lower impurity content being responsible. This possibility is considered remote, however, because any residual chlorine should be depleted before the specimen reached steady-state ablation. Even in the unlikely event that chlorine inhibition did play a role, the present results would still be applicable to the usual practical situation because purification of graphite

is conventionally accomplished with chlorination. Because chlorine has the desirable effect of inhibiting carbon oxidation, it would be particularly attractive for study in itself.

Effects of Crystallite Orientation

In figures 6 and 7 are graphically presented the pertinent data from table II which demonstrate the effects of crystallite orientation on ablation behavior. Figure 6 presents the data for those graphites which were tested while in thermal contact with the water-cooled holder, whereas figure 7 presents the data for those graphites tested while insulated from the holder. Comparisons of the ablation behavior for the different orientations of the graphites are made in terms of Δl, $\dot{m}$, and T_s and the two orientations are identified as A/G or W/G as before. Most of the graphites were tested in both the standard and purified forms.

The effects of crystallite orientation for those graphites which eroded evenly and were mounted directly in the water-cooled holder are seen in figures 6(a) to 6(h). These effects are smaller and not as obvious as those arising from differences in chemical impurity content. In these plots most of the data indicate a tendency for higher values of Δl and $\dot{m}$ in the A/G direction than in the W/G direction, although considerable overlap of the data sometimes exists. The L1 data (fig. 6(h)) show an apparent exception to this tendency, that is, $\dot{m}$ values in the W/G direction are slightly larger than those in the A/G direction. But, contradictorily, the Δl values are slightly larger in the A/G direction. It is believed, however, that the Δl values more likely indicate the true effect, if any, because they result from more direct measurements than the $\dot{m}$ values.

Considering the effect of crystallite orientation on T_s as shown in figures 6(a) to 6(h), there is little question that a higher T_s is reached in the A/G direction. This result is consistent with Δl and $\dot{m}$ also being higher. The largest temperature difference noted was about 5 percent (or 100° K).

Since the edges of a graphite crystallite are reportedly more reactive with oxygen than the faces (see, for instance, ref. 2), erosion in the W/G direction might be expected to be faster. This apparent contradiction to the present results is easily resolved, however, when it is recognized that thermal conductivity also depends on crystallite orientation and that it is highest in the W/G direction. Since the specimens were mounted in a water-cooled holder (an effective heat sink), the higher thermal conductivity in the W/G direction resulted in T_s being lower, and this lower T_s resulted in a lower Δl and $\dot{m}$. Evidently the tendency for the reaction to be faster in that direction because of the preferential exposure of crystallite edges was masked by the temperature dependence of the reaction rate.

To determine the magnitude of the difference in reactivity in the A/G and W/G directions at a common T_s, several specimens were tested while insulated from their

holders. The data for these tests are presented in figures 7(a) and 7(b). No longer are there any differences in T_s, Δl, or $\dot{m}$ for the two orientations. The fact that the erosion rates for both orientations are essentially the same implies that whatever difference in reactivity may exist between the edges and faces of the crystallites themselves is unimportant in affecting total erosion rate.

The ablation data for CDG, a graphite which eroded unevenly, are shown in figures 6(i) and 6(j). For this graphite, the effects of crystallite orientation are negligible, or at least the scatter in the data is such that no clear trends are discernible; this is true of T_s as well as of Δl and $\dot{m}$. However, as stated previously, a graphite such as this will have little, if any, practical usage for reentry applications, and consequently its lack of well-defined, reproducible behavior is of little practical concern.

The foregoing results indicate that for those graphites tested, crystallite orientation in itself has a negligible effect on ablation behavior provided the surface temperatures are the same. Extension of this result to other artificial graphites seems reasonable as long as they are not considerably more oriented than the graphites tested in this study. On the other hand, the ablation behavior of an artificial graphite can vary with crystallite orientation if the conditions of the application are such that thermal conduction from the graphite can occur to an extent sufficient to affect its surface temperature. The magnitude of the effect will, of course, depend on the degree of crystal anisotropy of the particular artificial graphite.

A comparison of the erosion rates of ATJ and ATJS can be made from the data in figures 4(a) to 4(d), 5(a) and 5(b), and 6(a) to 6(d). These data indicate that both the standard and purified forms of ATJ erode at a faster rate than the corresponding standard and purified forms of ATJS.

Comparisons With Diffusion-Controlled Predictions

From analysis of the present data, it becomes apparent that the erosion rate of artificial graphite at the present test conditions is not controlled by the diffusion of oxygen to the reacting surface, nor is this rate nearly as high as predicted by diffusion-control theory. This is in spite of the fact that the present test conditions are well within the range proposed by Scala as being diffusion controlled (ref. 10). This lack of diffusion control is evident from the fact that chemical impurities in a graphite increase its erosion rate and that surface-temperature differences arising from differences in crystallite orientation lead to differences in erosion rate. The dependence of erosion rate on temperature is shown in figure 8, in which the data for each graphite tested are plotted on an Arrhenius plot. The predicted diffusion-controlled rate limit of Scala (ref. 10) and the

somewhat lower predicted limit of Miller and Sutton (ref. 11) are shown for comparison.[1] Mass loss rates predicted by Scala's "slow" kinetics are considerably larger than these diffusion-controlled predictions. For instance, at $\frac{1}{T_s} = 5.6 \times 10^{-4}\ ^{o}K^{-1}$ ($T_s = 1785^{o}$ K), the mass loss rate is predicted to be 0.16 g/cm^{2}sec, well off the top of the graph.

In figure 8, the values of $\dot{m}$ for those graphites which eroded evenly cluster about a general trend line with temperature, whereas the data for those graphites which eroded unevenly are scattered with no apparent trend. To emphasize the trend of $\dot{m}$ for those graphites which eroded evenly, a dash line has been drawn by inspection through the data. From this line, an apparent activation energy for the erosion process was calculated to be about 30 kJ/mole. This value is considerably lower than the activation energies often associated with the carbon-oxygen reaction. For instance, Scala (ref. 10) cites a body of literature values between 75 kJ/mole and 185 kJ/mole and selects 180 kJ/mole as the most representative. On the other hand, the present value of 30 kJ/mole is much higher than that expected for a diffusion-controlled process, the activation energy of which should approach zero. It is possible, therefore, that the graphite erosion process at the present test conditions is neither strictly chemically controlled nor strictly diffusion controlled but is in an intermediate, or transition, regime. (Day, Walker, and Wright (ref. 13) reached a similar conclusion upon obtaining apparent activation energies between roughly 10 kJ/mole and 33 kJ/mole for the oxidation of carbon in a dynamic system at a pressure of 1 atm and at surface temperatures in the same range as those of the present study.) But, although the assumption of the present erosion process being in a transition regime would explain the low apparent activation energy, it is not simultaneously consistent with the fact that the data are far below (roughly one-half) the predicted diffusion-controlled limit. For diffusion to have much effect on the oxidation process (i.e., for the process to be in a transition regime) the predicted diffusion limit would have to be considerably lower.

There are reasons other than the process being in a transition regime, however, which could account for the low apparent activation energy. One of these is that in addition to the oxidative removal of mass, some mass is also very likely lost in the form of discrete particles as a result of mechanical and aerodynamic forces (ref. 9). Such particle removal is more easily observed for those graphites which eroded unevenly, but it

[1]The diffusion limits shown in figure 8 are for a 0.635-cm-nose-radius body, the initial geometry of the specimens. However, by using the method of reference 12 and the photographs of the specimens in figure 3, effective nose radii can be calculated which enable adjustment of these diffusion limits for the actual shapes attained by the specimens during test. According to such calculations, the diffusion limits for the ATJ, ATJS, and L1 specimens should be somewhat lower – approximately 0.046 g/cm^{2}sec for reference 10 or 0.040 g/cm^{2}sec for reference 11. The diffusion limits for ATL and CDG should be higher by a factor of between $1\frac{1}{2}$ and 2; however, these limits are of little significance since a large part of the total erosion rates of these specimens is due to particle removal in addition to oxidative removal.

very likely also occurs to some extent from those graphites which eroded evenly. Since particle removal should be largely dependent on the pressure and flow field, but dependent on temperature only to the small extent that it may be linked with oxidation, a contribution of particle removal to the total erosion process will lower the apparent activation energy of the process below that of pure oxidation. Such particle removal could not, however, by itself account for the observed mass loss rates being lower than diffusion-controlled predictions. Accordingly, particle removal does not seem to be a likely explanation.

One intriguing possible solution to this apparent contradiction may be that the true activation energy of the oxidation process itself is lower at the present test conditions than assumed by Scala. That this may actually be the case is not without foundation. For instance, a number of authors (refs. 14 to 18) have published experimental data obtained with great care to minimize or eliminate diffusional complications. These data indicate that the oxidation rate of carbon passes through a maximum with increasing temperature, the maximum occurring in the temperature range from 1500° K to 2300° K depending on the carbon type and the test conditions. Moreover, such a maximum has been demonstrated to be possible solely on the basis of theoretical thermochemical and kinetic considerations (ref. 19). In view of these reported results it is not entirely improbable that the low apparent activation energy of the present process might simply be a manifestation of a decrease in true activation energy of the oxidation process at higher temperatures. To establish or disprove this point would require a separate comprehensive study in itself, but since a commonly accepted theory of high-temperature ablation of graphite would be markedly affected were it proven to be true, such a study seems to be justified.

Also of interest from the present data is the implication that for a given artificial graphite at a given impurity level and at the test conditions of this study, $\dot{m}$ is a function largely of T_s alone, being virtually independent of the level of heat flux and thermal conduction from the graphite specimen and of crystallite orientation. This suggests that mass loss rate is independent of temperature distribution and heat-flow path within the specimen which, in turn, implies that the ablation process is largely a surface phenomenon.

Although incidental to the main purpose of the present investigation, one might reasonably ask if there is any significance to the fact that the graphites which reached the highest temperatures also eroded unevenly (see fig. 8). To answer this question, one specimen of CDG was tested at an intentionally very low heating rate to produce a low surface temperature. The surface temperature obtained was 1730° K $\left(\frac{1}{T_s} = 5.8 \times 10^{-4}\ {}^{\circ}K^{-1}\right)$, at which temperature the graphite still eroded unevenly with considerable particle removal and the mass loss rate was virtually the same as for the other CDG specimens. This test indicates that it is not necessary for a graphite to reach a surface temperature above

2220^{o} K $\left(\text{i.e., } \frac{1}{T_s} \text{ less than } 4.5 \times 10^{-4}\ {}^{o}K^{-1}\right)$ for particle removal to occur and, furthermore, that particle removal is more a function of the particular graphite than of the surface temperature.

CONCLUSIONS

The effects of natural chemical impurities and crystallite orientation on the erosion behavior of several artificial graphites have been determined in a representative reentry environment. Some of the graphites tested eroded evenly and smoothly, whereas others eroded unevenly and produced rough, pitted surfaces. The conclusions of this study are listed as follows:

1. The presence of natural chemical impurities in an artificial graphite can result in a higher total recession Δl, a higher mass loss rate $\dot{m}$, and a higher surface temperature T_s than when the impurities are not present. The largest effects observed in this study were increases of about 20 percent for Δl, about 20 percent for $\dot{m}$, and about 10 percent (or 200^{o} K) for T_s.

2. Crystallite orientation has a negligible effect on the erosion rate of artificial graphite provided T_s is the same for both orientations.

3. Since the thermal conductivity of artificial graphite varies with orientation, differences in orientation can affect erosion behavior when a heat sink is in contact with the graphite. (Higher surface temperatures will be reached when the test stream impinges on the graphite in the across-grain direction.) The largest temperature differences observed in this study were about 5 percent (100^{o} K). Accompanying the higher surface temperatures were slightly higher values of Δl and $\dot{m}$. No effect of orientation was observed for those graphites which eroded unevenly.

4. The graphite erosion rates measured in the present study are significantly slower than those predicted by accepted diffusion-control theory and, furthermore, show a temperature dependence which does not conform to strict diffusion-control concepts.

5. An apparent activation energy for the erosion process was calculated from the present data to be about 30 kJ/mole (about 1/3 to 1/6 of the activation energies commonly reported for oxidation); also, erosion rates were roughly half of those predicted by diffusion-control theory. One possibility which could account for both of these phenomena is that at the present test conditions the oxidation reaction has a lower true activation energy than has often been assumed in ablation calculations.

6. For any given graphite and impurity level, and at the test conditions of this study, the ablation process is largely a surface phenomenon, the mass loss rate being virtually a function of T_s alone.

7. The standard and purified forms of ATJ erode at a faster rate at a given surface temperature than the corresponding standard and purified forms of ATJS.

Langley Research Center,
National Aeronautics and Space Administration,
Hampton, Va., September 3, 1970.

REFERENCES

1. Maahs, Howard G.; and Schryer, David R.: Chemical Impurity Data on Selected Artificial Graphites With Comments on the Catalytic Effect of Impurities on Oxidation Rate. NASA TN D-4212, 1967.

2. Maahs, Howard G.: Crystallographic Data on Selected Artificial Graphites With Comments on the Role of the Degree of Crystal Development in Oxidation. NASA TN D-4888, 1968.

3. Mayo, Robert F.; Wells, William L.; and Wallio, Milton A.: A Magnetically Rotated Electric Arc Air Heater Employing a Strong Magnetic Field and Copper Electrodes. NASA TN D-2032, 1963.

4. Fay, J. A.; and Riddell, F. R.: Theory of Stagnation Point Heat Transfer in Dissociated Air. J. Aeronaut. Sci., vol. 25, no. 2, Feb. 1958, pp. 73-85, 121.

5. Bacon, G. E.: A Method for Determining the Degree of Orientation of Graphite. J. Appl. Chem. (London), vol. 6, 1956, pp. 477-481.

6. Exton, Reginald J.: Theory and Operation of a Variable Exposure Photographic Pyrometer Over the Temperature Range 1800^{o} to 3600^{o} F (1255^{o} to 2255^{o} K). NASA TN D-2660, 1965.

7. Wilson, R. Gale; and Spitzer, Cary R.: High-Temperature Spectral Emittance of Ablation Chars and Carbon From 0.4 to 2.4 Micrometers. AIAA Pap. No. 67-326, Apr. 1967.

8. Null, M. R.; and Lozier, W. W.: Research and Development on Advanced Graphite Materials – Vol. XXI. Carbon Arc Image Furnace Studies of Graphite. WADD-TR-61-72, Vol. XXI, U.S. Air Force, Nov. 1963. (Available from DDC as AD No. 426 665.)

9. Maahs, Howard G; and Schryer, David R.: Particle Removal in the Ablation of Artificial Graphite. AIAA J., vol. 7, no. 11, Nov. 1969, pp. 2178-2179.

10. Scala, Sinclaire M.: The Ablation of Graphite in Dissociated Air. Pt. I: Theory. R62SD72, Missile and Space Div., Gen. Elec. Co., Sept. 1962.

11. Miller, Irvin M.; and Sutton, Kenneth: An Experimental Study of the Oxidation of Graphite in High-Temperature Supersonic and Hypersonic Environments. NASA TN D-3444, 1966.

12. Zoby, Ernest V.; and Sullivan, Edward M.: Effects of Corner Radius on Stagnation-Point Velocity Gradients on Blunt Axisymmetric Bodies. NASA TM X-1067, 1965.

13. Day, R. J.; Walker, P. L.; and Wright, C. C.: The Carbon-Oxygen Reaction at High Temperatures and High Gas Flow Rates. Conference on Industrial Carbon and Graphite, Soc. Chem. Ind. (London), 1958, pp. 348-370.

14. Nagle, J.; and Strickland-Constable, R. F.: Oxidation of Carbon Between 1000-2000°C. Proceedings of the Fifth Conference on Carbon, Vol. 1, Pergamon Press, Inc., 1962, pp. 154-164.

15. Walls, J. R.; and Strickland-Constable, R. F.: Oxidation of Carbon Between 1000-2400°C. Carbon, vol. 1, no. 3, Apr. 1964, pp. 333-338.

16. Rosner, D. E.; and Allendorf, H. D.: High Temperature Oxidation of Carbon by Atomic Oxygen. Carbon, vol. 3, no. 2, Oct. 1965, pp. 153-156.

17. Rosner, Daniel E.; and Allendorf, H. Donald: Comparative Studies of the Attack of Pyrolytic and Isotropic Graphite by Atomic and Molecular Oxygen at High Temperatures. AIAA J., vol. 6, no. 4, Apr. 1968, pp. 650-654.

18. Lewis, J. C.; Floyd, I. J.; and Cowlard, F. C.: A Comparative Study of the Gaseous Oxidation of Vitreous Carbon and Various Graphites at 1500-3000°K. Paper presented at Eighth Biennial Conference on Carbon (Buffalo, N.Y.), June 1967.

19. Ong, J. N., Jr.: On the Kinetics of Oxidation of Graphite. Carbon, vol. 2, no. 3, Dec. 1964, pp. 281-297.

TABLE I.- GRAPHITES TESTED

Graphite grade	Supplier (a)	Purity (b)	Ash content, ppm	Total impurities, ppm	Filler carbon (c)	Maximum grain size, mm	Bulk density, g/cc	Anisotropy ratio
ATJ	UC	Std	1209	460	PC	0.15	1.72	0.48
		Pure	25	30	PC	.15	1.71	.38
ATJS	UC	Std	1625	307	PC	.15	1.84	.42
		Pure	<5	22	PC	.15	1.83	.48
ATL	UC	Std	5810	3585	PC	.76	1.79	(d)
		Pure	17	22	PC	.76	1.78	(d)
CDG	UC	Std	531	179	PC,LB	.41	1.50	.59
		Pure	<5	22	PC,LB	.41	1.49	.59
L1	SC	Std	709	410	PC	.15	1.54	.30

[a]Suppliers are: UC, Union Carbide Corporation; SC, Stackpole Carbon Company.

[b]Purity designations: Std, as conventionally supplied; Pure, specially purified.

[c]Filler materials are: LB, lampblack; PC, petroleum coke.

[d]Not measured.

TABLE II.- ABLATION BEHAVIOR

Graphite grade	Heating rate, q_{cw}, W/cm^2	Orientation (a)	Purity (b)	Total recession in 30 sec, Δl, cm	Mass loss rate, $\dot{m}$, g/cm^2sec	Surface temperature, T_s, ^oK
Data obtained without insulation						
ATJ	530	A/G	Std	0.4211	0.02826	2170
				.4346	.03120	2165
				.4514	.03150	2190
				.4201	.03023	2155
			Pure	0.3622	0.02441	1965
				.3668	.02428	1975
				.3627	.02527	1980
		W/G	Std	0.4247	0.03025	2080
				.3884	.02709	2040
				.3919	.02832	2055
				.4054	.02785	2060
			Pure	0.3160	0.02115	1820
				.3533	.02433	1890
				.3358	.02253	1880
ATJS	530	A/G	Std	0.4001	0.02737	2155
				.4112	.03007	----
				[c].4074	[c].02912	[c]2165
			Pure	[c]0.3376	[c]0.02824	[c]2035
				[c].3457	[c].02517	[c]2045
				.3142	.02223	1890
		W/G	Std	0.3785	0.02701	2070
				.3594	-----	2095
				[c].3825	[c].02848	[c]2175
			Pure	[c]0.3254	[c]0.02508	[c]1955
				[c].3198	[c].02273	[c]1950
				.2350	.02165	1770
ATJS	655	A/G	Pure	0.3787	0.02537	2070
				.3696	.02389	2040
				.3734	.02382	2055
		W/G	Pure	0.3599	0.02440	1965
				.3536	.02464	1945
				.3564	.02324	1930
[d]CDG	550	A/G	Std	[e]0.5159	0.03938	2330
				[e].4986	.04588	2335
				.8603	.04940	2310
			Pure	[e]0.4752	0.03825	2250
				[e].3813	-----	2250
				.7699	.04066	2260
		W/G	Std	[e]0.5494	.04499	2335
				[e].5022	.03977	2280
				.8946	-----	2300
			Pure	[e]0.4910	0.03872	2230
				[e].5517	.04980	2260
				.7615	.04356	2220
L1	550	A/G	Std	0.5019	0.02755	2175
				.4983	.02391	2160
				.5138	.02545	2200
		W/G	Std	0.4912	0.02853	2095
				.4864	.02608	2060
				.5017	.02881	2045

[a]Crystallite orientations: A/G, across grain; W/G, with grain.

[b]Purity designations: Std, as conventionally supplied; Pure, specially purified.

[c]Gap between the specimen and its holder.

[d]Eroded unevenly, yielded a rough, pitted surface.

[e]20-second test.

TABLE II.- ABLATION BEHAVIOR – Concluded

Graphite grade	Heating rate, q_{cw}, W/cm^2	Orientation (a)	Purity (b)	Total recession in 30 sec, Δl, cm	Mass loss rate, $\dot{m}$, $g/cm^2 sec$	Surface temperature, T_s, ^oK
Data obtained with insulation						
ATJ	535	A/G	Std	0.4533	0.02999	2155
				.4569	.02955	2200
				.4666	.03272	2190
		W/G	Std	0.4498	0.03111	2180
				.4658	.03132	2180
				.4592	.03292	2185
L1	535	A/G	Std	0.4956	0.02883	2120
				.5034	.02814	2070
				.5108	.02703	2145
		W/G	Std	0.4945	0.02819	2060
				.5278	.02845	2080
				.4729	.02823	2060
ATJ	515	A/G	Std	0.4559	0.02949	2200
			Pure	0.3835	0.02703	2140
ATJS	515	A/G	Std	0.3985	0.02817	2160
			Pure	0.3668	0.02641	2060
[d]ATL	515	A/G	Std	0.6607	0.03747	2300
				.6706	.04682	----
			Pure	0.7142	0.05456	2255
[d]CDG	515	A/G	Std	0.9385	0.04247	2210
			Pure	0.7435	0.03333	2180

[a]Crystallite orientations: A/G, across grain; W/G, with grain.

[b]Purity designations: Std, as conventionally supplied; Pure, specially purified.

[d]Eroded unevenly, yielded a rough, pitted surface.

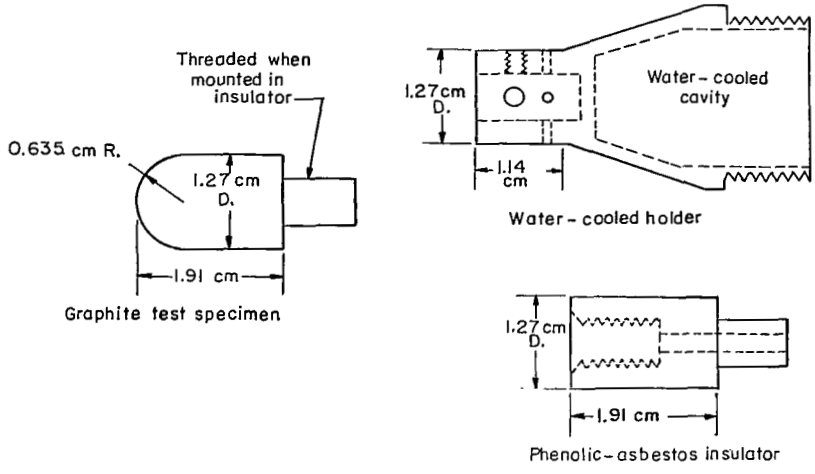

Figure 1.- Schematic showing graphite test specimen, water-cooled holder, and insulator.

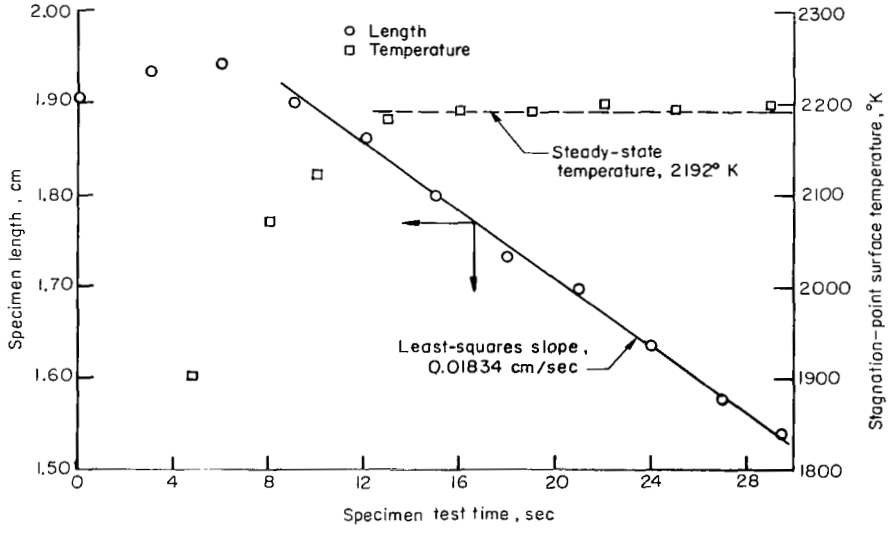

Figure 2.- Sample plot of length and surface temperature as a function of time.

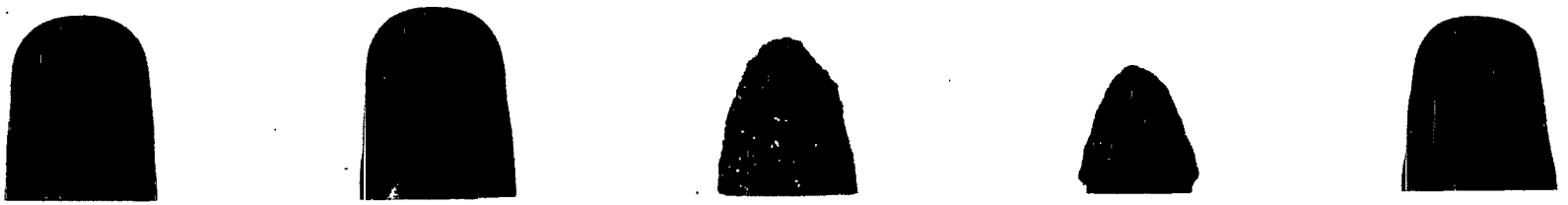

L-70-4762

Figure 3.- Photograph of graphite specimens after test.

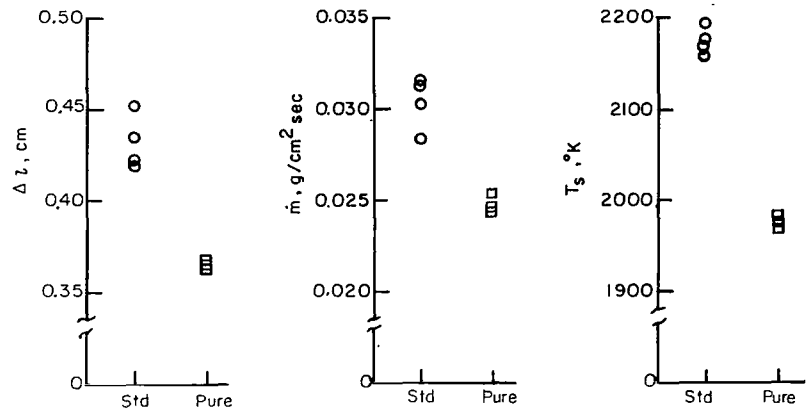

(a) ATJ (A/G); q_{cw} = 530 W/cm^2.

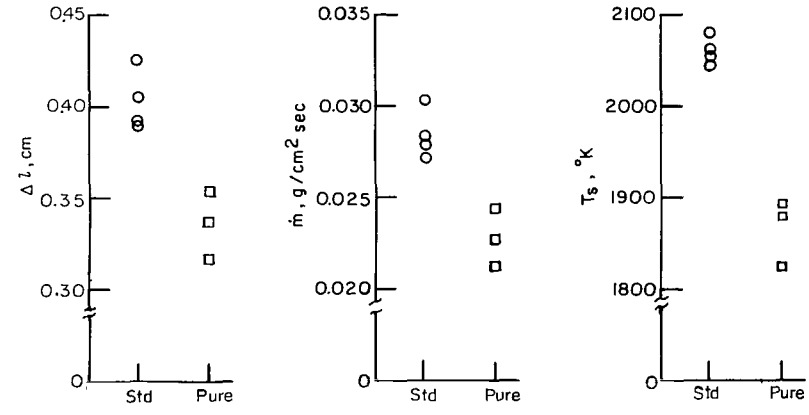

(b) ATJ (W/G); q_{cw} = 530 W/cm^2.

Figure 4.- Effect of natural chemical impurities on ablation behavior. Model uninsulated.

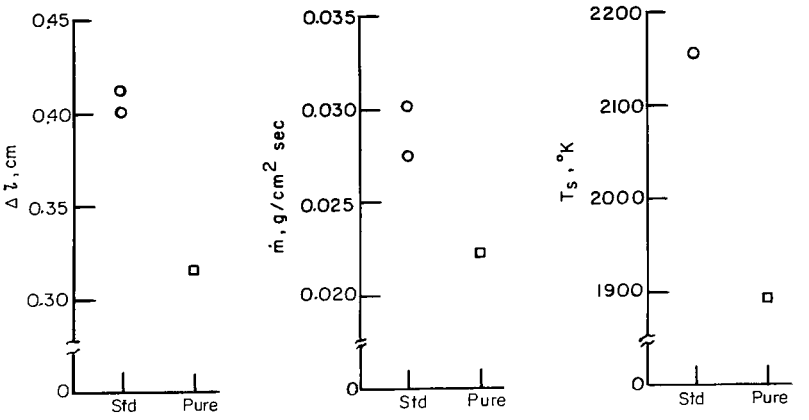

(c) ATJS (A/G); q_{cw} = 530 W/cm^2.

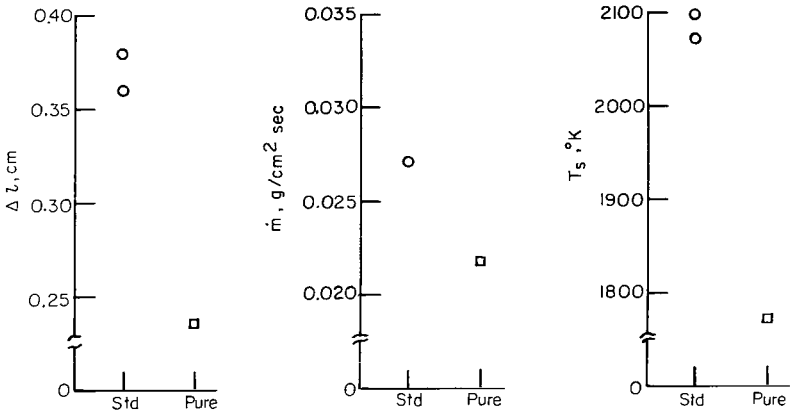

(d) ATJS (W/G); q_{cw} = 530 W/cm^2.

Figure 4.- Continued.

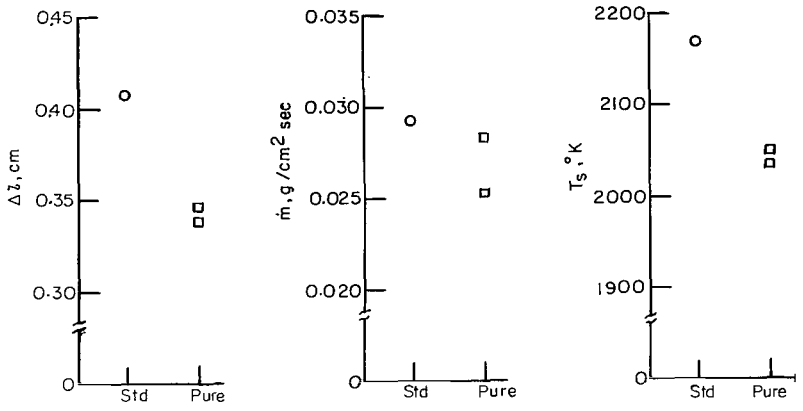

(e) ATJS (A/G); q_{cw} = 530 W/cm^2; gap between specimen and its holder.

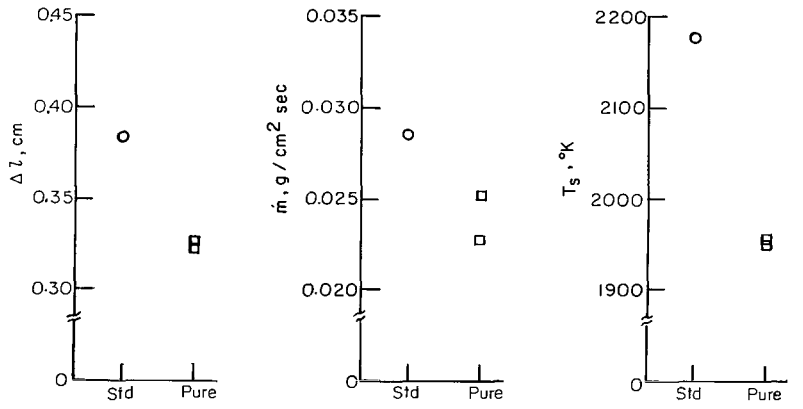

(f) ATJS (W/G); q_{cw} = 530 W/cm^2; gap between specimen and its holder.

Figure 4.- Continued.

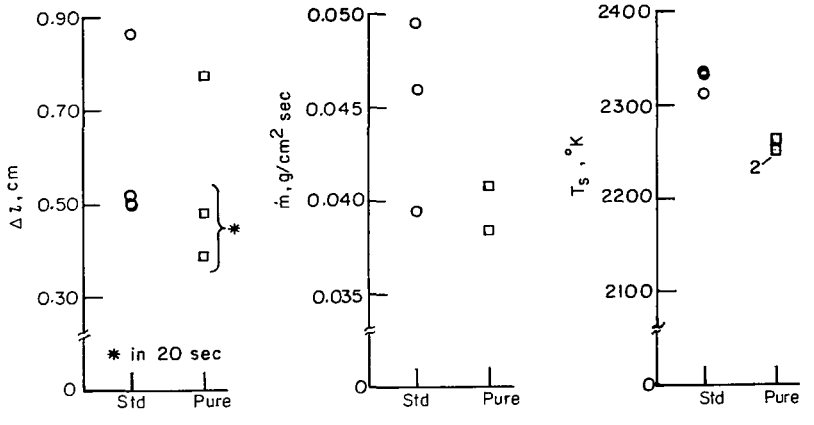

(g) CDG (A/G); q_{cw} = 550 W/cm^2.

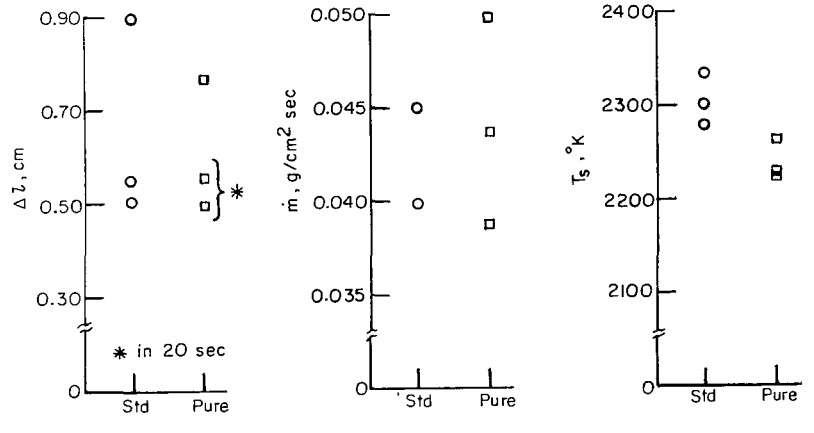

(h) CDG (W/G); q_{cw} = 550 W/cm^2.

Figure 4.- Concluded.

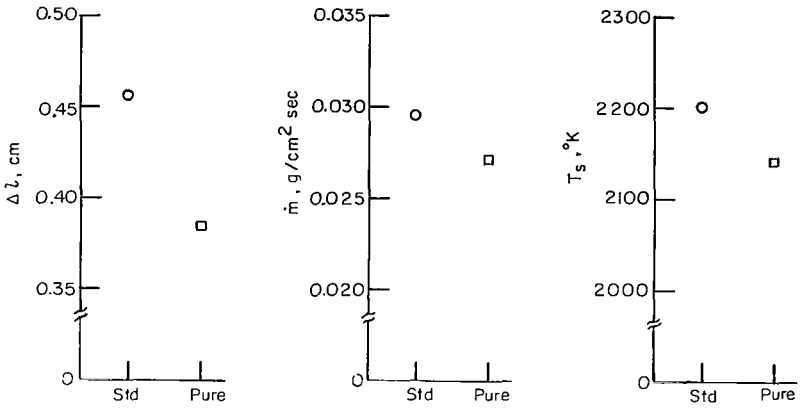

(a) ATJ (A/G); q_{cw} = 515 W/cm^2.

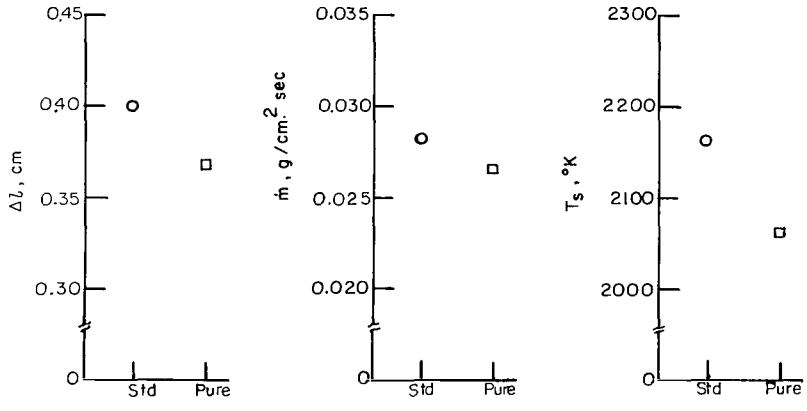

(b) ATJS (A/G); q_{cw} = 515 W/cm^2.

Figure 5.- Effect of natural chemical impurities an ablation behavior. Model insulated.

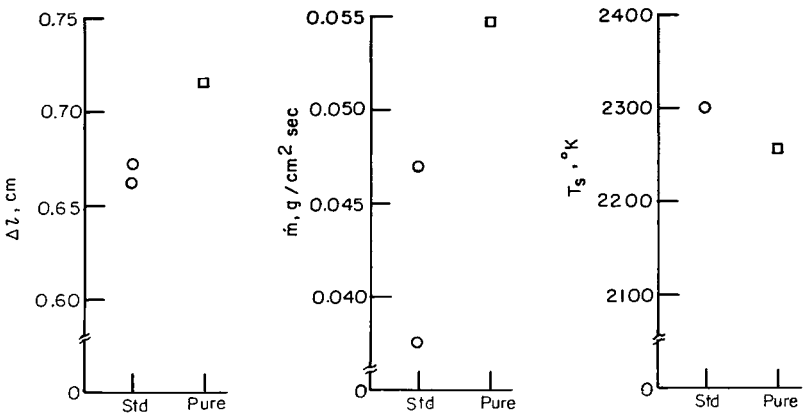

(c) ATL (A/G); q_{cw} = 515 W/cm^2.

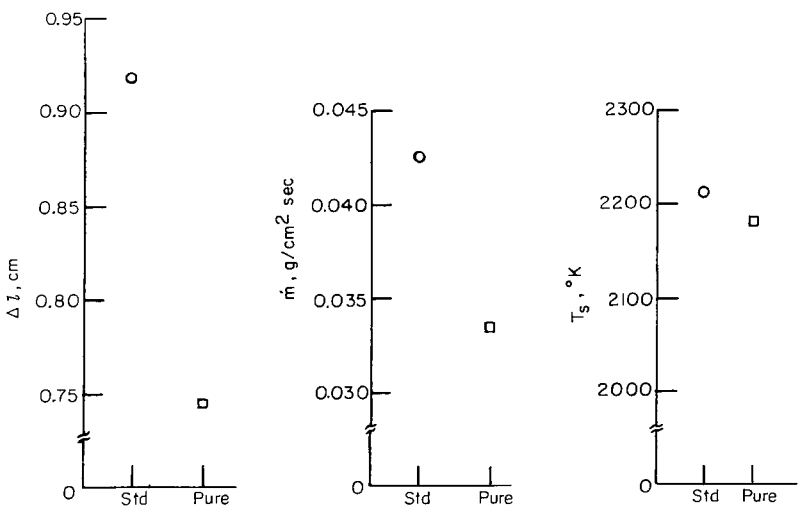

(d) CDG (A/G); q_{cw} = 515 W/cm^2.

Figure 5.- Concluded.

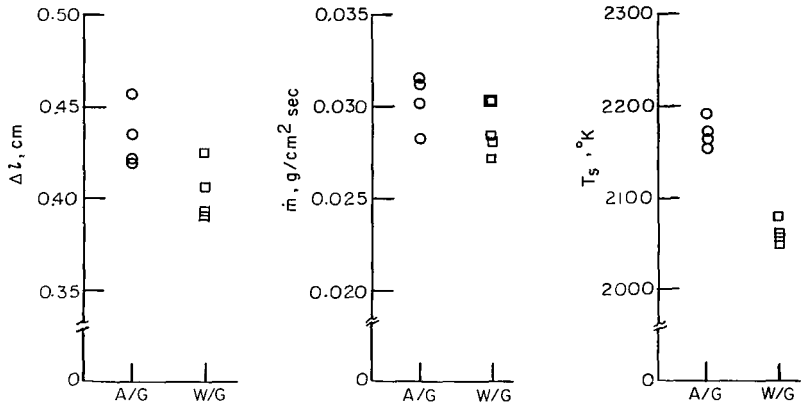

(a) ATJ (Std); q_{cw} = 530 W/cm^2.

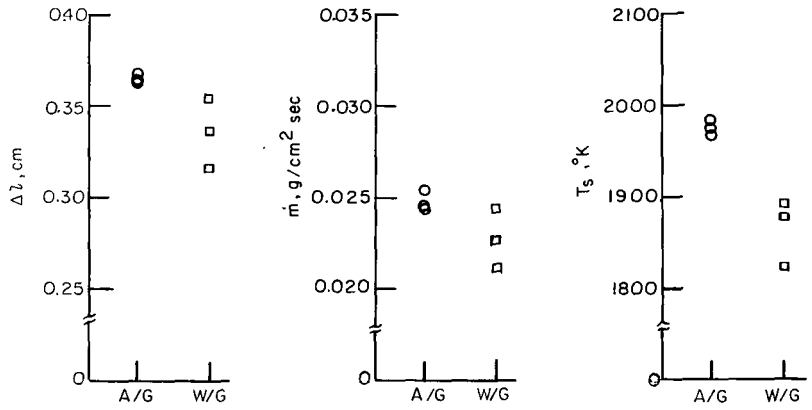

(b) ATJ (Pure); q_{cw} = 530 W/cm^2.

Figure 6.- Effect of crystallite orientation on ablation behavior. Model uninsulated.

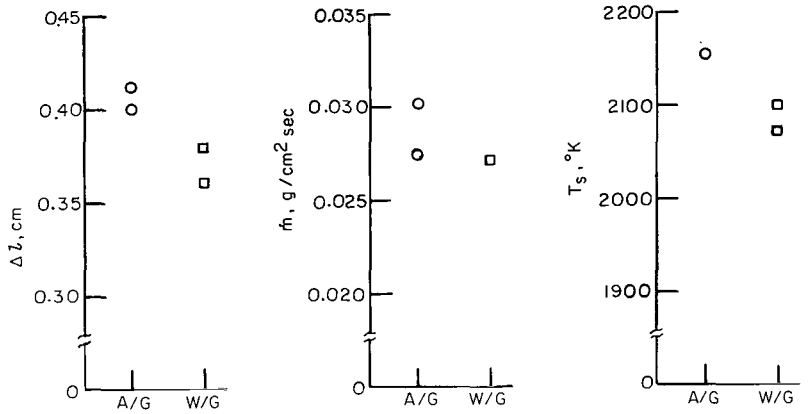

(c) ATJS (Std); q_{cw} = 530 W/cm^2.

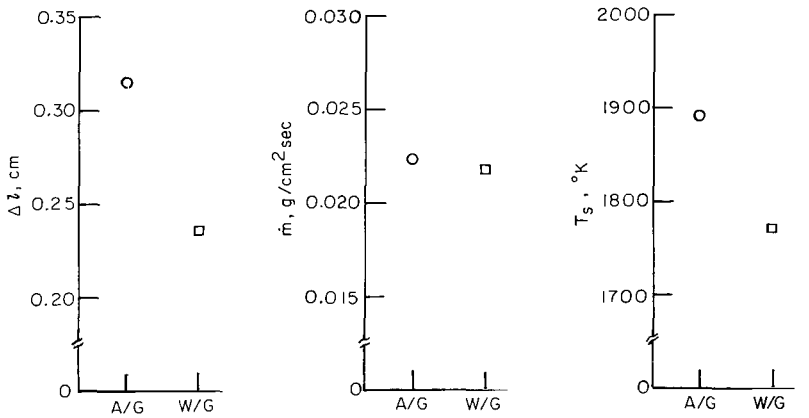

(d) ATJS (Pure); q_{cw} = 530 W/cm^2.

Figure 6.- Continued.

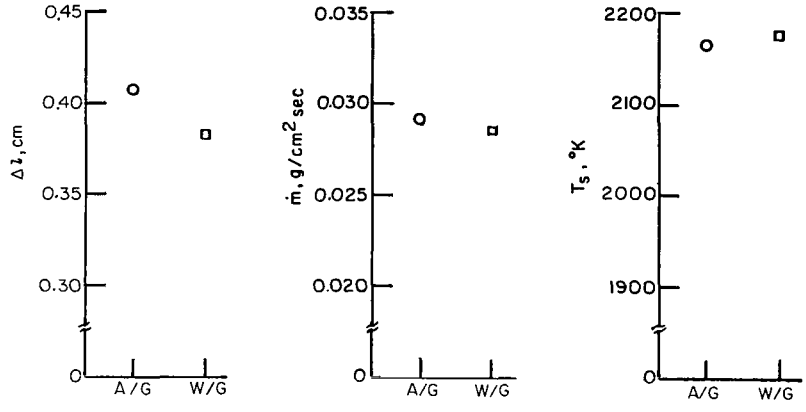

(e) ATJS (Std); q_{cw} = 530 W/cm^2; gap between specimen and its holder.

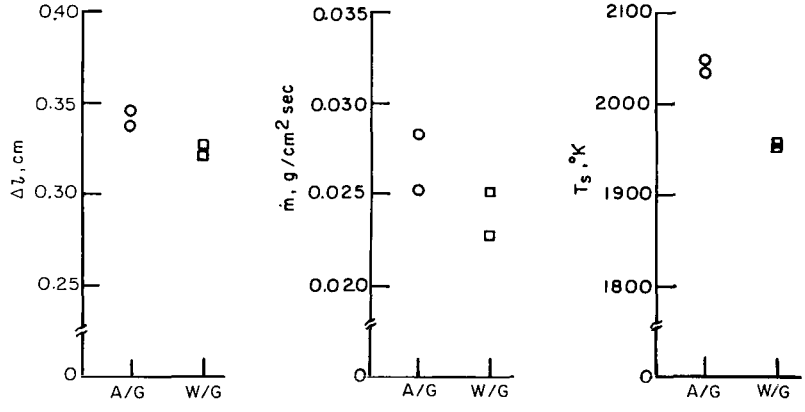

(f) ATJS (Pure); q_{cw} = 530 W/cm^2; gap between specimen and its holder.

Figure 6.- Continued.

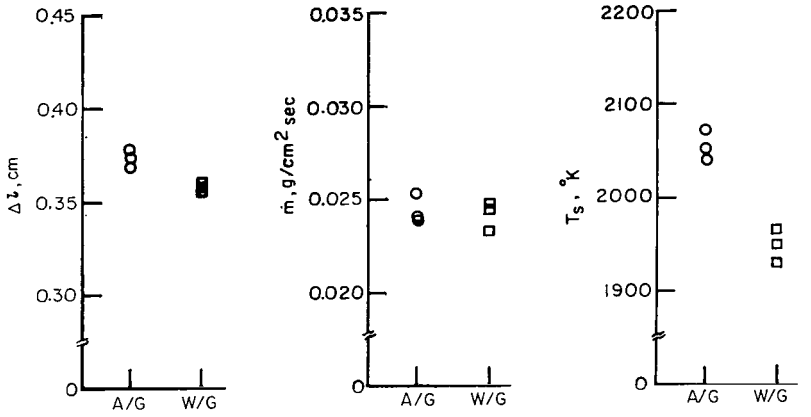

(g) ATJS (Pure); q_{cw} = 655 W/cm^2.

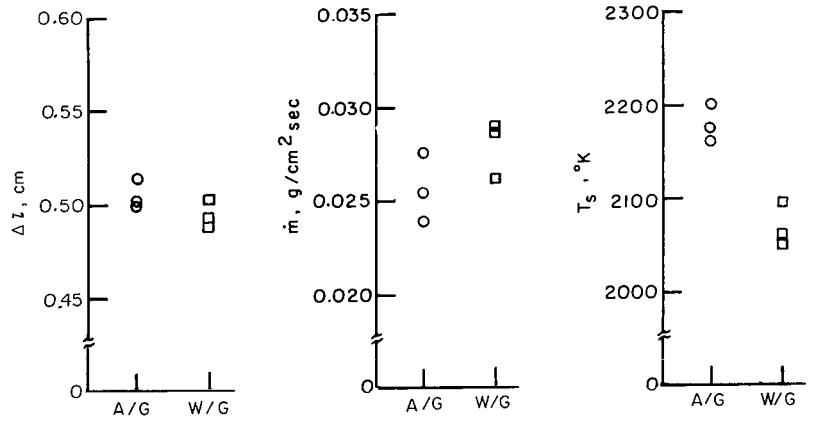

(h) L1 (Std); q_{cw} = 550 W/cm^2.

Figure 6.- Continued.

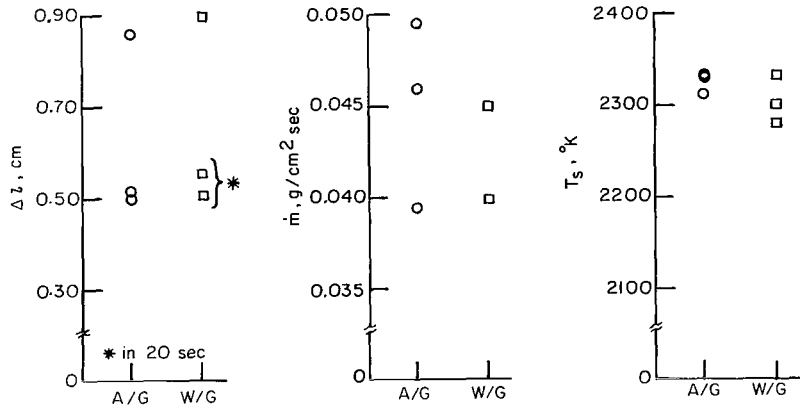

(i) CDG (Std); q_{cw} = 550 W/cm^2.

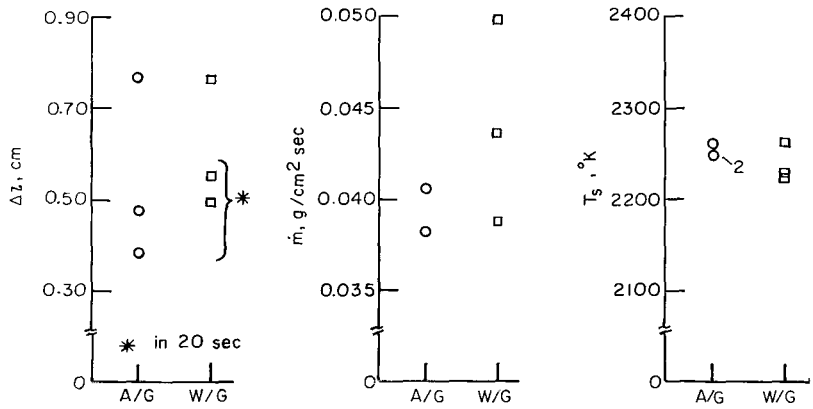

(j) CDG (Pure); q_{cw} = 550 W/cm^2.

Figure 6.- Concluded.

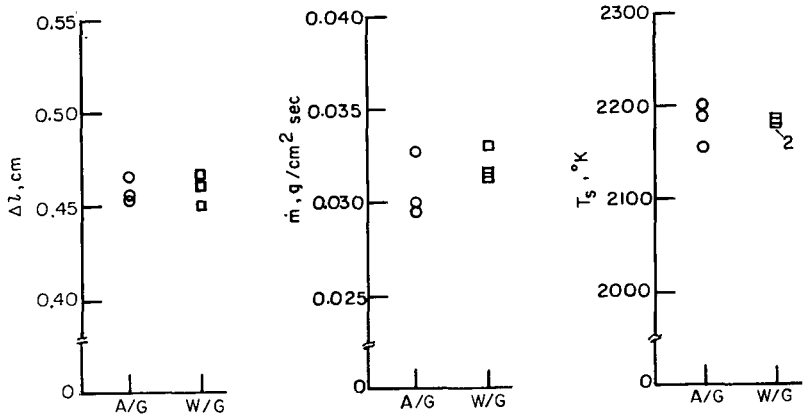

(a) ATJ (Std); q_{cw} = 535 W/cm^2.

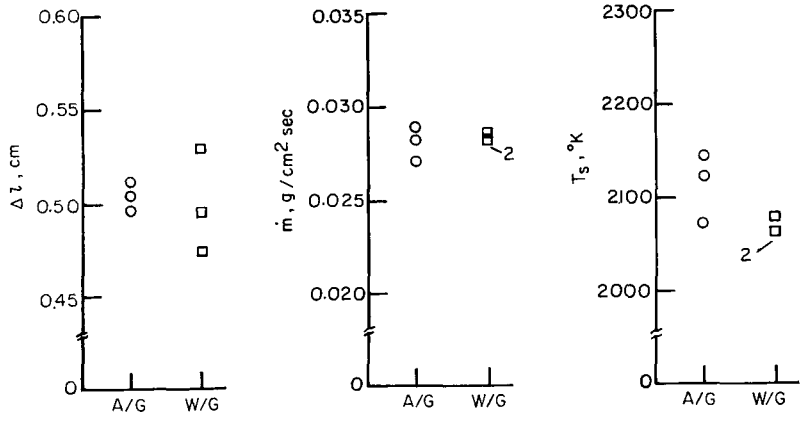

(b) L1 (Std); q_{cw} = 535 W/cm^2.

Figure 7.- Effect of crystallite orientation on ablation behavior. Model insulated.

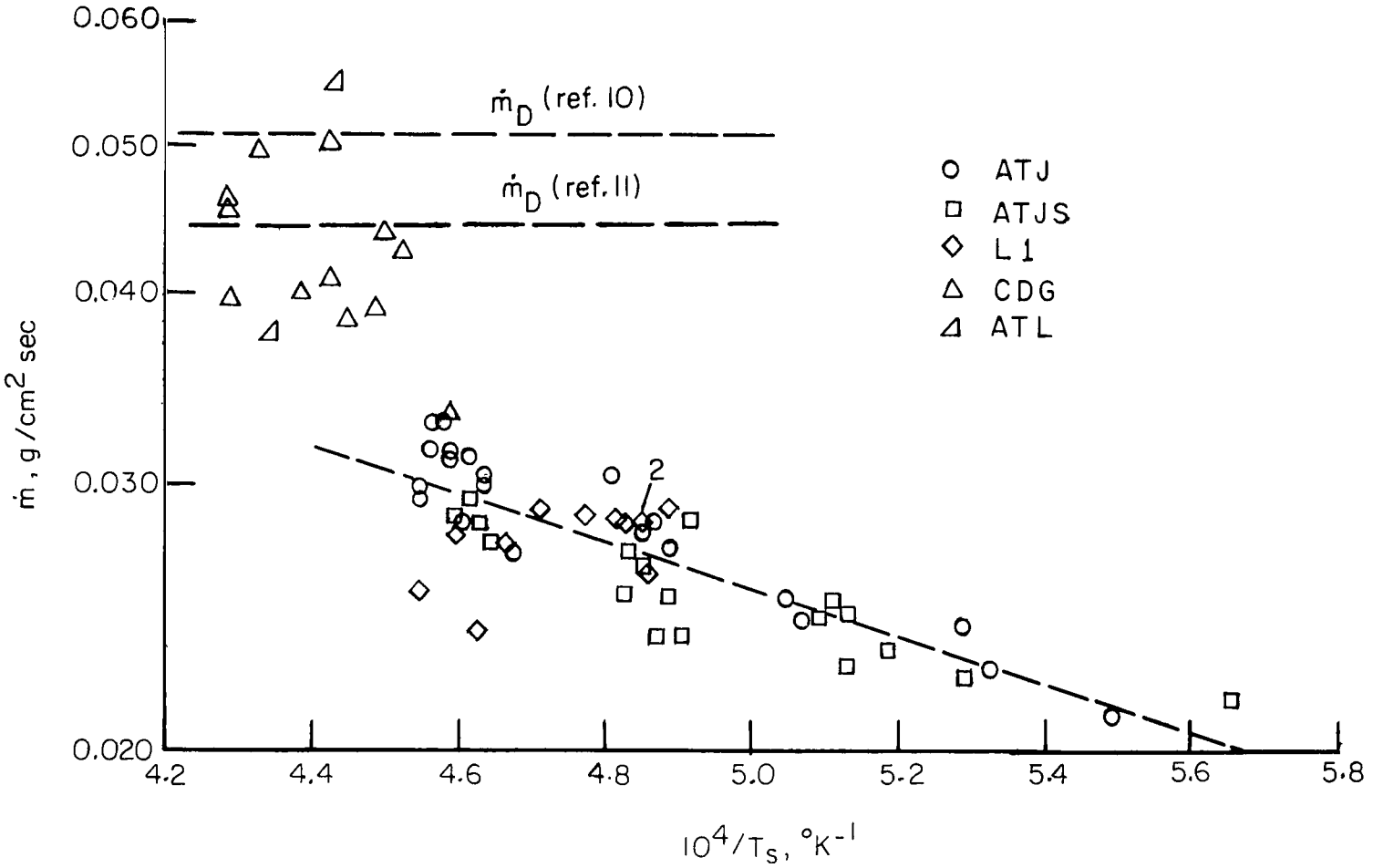

Figure 8.- Linear mass loss rate as function of inverse stagnation-point surface temperature.

"The aeronautical and space activities of the United States shall be conducted so as to contribute . . . to the expansion of human knowledge of phenomena in the atmosphere and space. The Administration shall provide for the widest practicable and appropriate dissemination of information concerning its activities and the results thereof."

—NATIONAL AERONAUTICS AND SPACE ACT OF 1958

NASA SCIENTIFIC AND TECHNICAL PUBLICATIONS

TECHNICAL REPORTS: Scientific and technical information considered important, complete, and a lasting contribution to existing knowledge.

TECHNICAL NOTES: Information less broad in scope but nevertheless of importance as a contribution to existing knowledge.

TECHNICAL MEMORANDUMS: Information receiving limited distribution because of preliminary data, security classification, or other reasons.

CONTRACTOR REPORTS: Scientific and technical information generated under a NASA contract or grant and considered an important contribution to existing knowledge.

TECHNICAL TRANSLATIONS: Information published in a foreign language considered to merit NASA distribution in English.

SPECIAL PUBLICATIONS: Information derived from or of value to NASA activities. Publications include conference proceedings, monographs, data compilations, handbooks, sourcebooks, and special bibliographies.

TECHNOLOGY UTILIZATION PUBLICATIONS: Information on technology used by NASA that may be of particular interest in commercial and other non-aerospace applications. Publications include Tech Briefs, Technology Utilization Reports and Notes, and Technology Surveys.

Details on the availability of these publications may be obtained from:

SCIENTIFIC AND TECHNICAL INFORMATION DIVISION

NATIONAL AERONAUTICS AND SPACE ADMINISTRATION

Washington, D.C. 20546